

Traces of wobbling accretion disk in X-ray pulsar Her X-1 from observations of the ART-XC telescope of the SRG observatory.

V. M. Revnivtsev^{1,2*}, K. A. Postnov¹, S. V. Molkov², N. I. Shakura¹, A. A. Lutovinov², I. Yu. Lapshov²,
D. A. Kolesnikov¹, A. Yu. Tkachenko²

¹ Moscow State University, Sternberg Astronomical Institute, 119234 Moscow, Russia

² Space Research Institute of the Russian Academy of Sciences, 117997 Moscow, Russia

June 12, 2025

ABSTRACT

Long uninterrupted observations of the X-ray binary system Her X-1 were performed with the Mikhail Pavlinsky ART-XC telescope of the Spectrum-Röntgen-Gamma (SRG) X-ray Observatory in the 4–25 keV energy range with a total exposure of about two days around the main turn-on of the X-ray source. We present the results of timing and spectral analysis of these observations. The opening of the X-ray source is determined to occur at the orbital phase $\phi_b \approx 0.25$. The analysis of the X-ray light curve reveals a first direct observational evidence of the nutation of a tilted precessing accretion disk with a period of ≈ 0.87 days. The appearance of X-ray pulsations near the orbital phase $\phi_b \approx 0.77$ prior to the main turn-on at the maximum of the nutation variability has been also detected. During the X-ray eclipse, a non-zero X-ray flux is measured, which is presumably associated with scattering of an X-ray emission in a hot corona around the optical star illuminated by the X-rays from the central neutron star. An increase in the X-ray flux after the main turn-on can be described by the passage of the radiation from the central source through a scattering corona above the precessing accretion disk.

Key words. X-rays: binaries – X-rays: individuals: Her X-1

1. Introduction

Her X-1/HZ Her is an eclipsing close X-ray binary system harboring a neutron star with a mass of $\approx 1.5M_\odot$ and the optical star HZ Her with a mass of $\approx 2M_\odot$. The HZ Her was known as a variable star with an unusually large optical variability. After the discovery of the X-ray pulsar Her X-1 and its optical identification with HZ Her, it became clear that it enters a binary system consisting of a normal star and a neutron star (Tananbaum et al. 1972; Giacconi et al. 1973). The large optical variability of HZ Her is a consequence of the heating of the normal star by the X-ray radiation of the neutron star (the reflection effect, Cherepashchuk et al. 1972; Gerend & Boynton 1976; Shakura et al. 2021).

An X-ray flux from Her X-1 demonstrates several characteristic periodicities: X-ray pulsations with the neutron star's spin period of $P_x \approx 1.24$ s; the variability with the binary orbital motion with a period of $P_b \approx 1.7$ days; the superorbital variability with a period of $P_{\text{prec}} \approx 35$ days. The 35-day period is caused by the precession of an accretion disk around the neutron star in the retrograde direction to the orbital motion. Because of the large orbital inclination of the binary system $i \approx 90$ degrees (Crampton & Hutchings 1974), the central X-ray source is periodically eclipsed both by the optical star and the inclined accretion disk. The precession period consists of two X-ray bright states: a bright main-on state (lasting about seven orbits) followed by a low state with almost zero X-ray flux (lasting about four orbits), and a shorter secondary short-on state with lower X-ray flux than in the main-on state (lasting about five orbits)

followed by the second low state (about four orbits). A detailed description of the phenomenology of the 35-day X-ray variability can be found in Shakura et al. (1998); Leahy & Wang (2020); Shakura et al. (2021). The X-ray luminosity of the source in the main-on state reaches $L_x \approx 10^{37}$ erg/s.

The accretion disk is the key element of the Her X-1 binary system that modulates the observed X-ray radiation. The shape and dynamics of the disk can be caused by the reaction of the asymmetrical coronal disk wind (Schandl & Meyer 1994), radiation reaction from the central luminous X-ray source (Wijers & Pringle 1999) or, alternatively, by a combination of tidal effects in the binary system and dynamical effects of accreting gas stream leading to the precession of the disk with a period of 35 days (Shakura et al. 1998).

As shown in Scott et al. (2000), phenomenologically, precession of a twisted tilted accretion disk around non-precessing neutron star is capable of explaining X-ray pulse profile changes in Her X-1. Alternatively, X-ray pulse profile changes can be explained by a model of freely precessing neutron star (Postnov et al. 2013). Recently, evidence for triaxial neutron star precession was found *Fermi*/GBM measurements of pulse period (Kolesnikov et al. 2022). Based on the RXTE observations, a model of a wobbling (nutating) accretion disk was proposed by Klochkov et al. (2006) to explain an anomalous appearance of the X-ray source during its low states, when the neutron star becomes visible for a short time to the observer.

Her X-1 has been observed many times by different X-ray observatories in various states (see e.g. Tananbaum et al. 1972; Lutovinov et al. 2000; Klochkov et al. 2008; Leahy & Wang 2020; Caiazzo et al. 2022; Leahy & Sharma 2024, and refer-

* vlad.revnivtsev@cosmos.ru

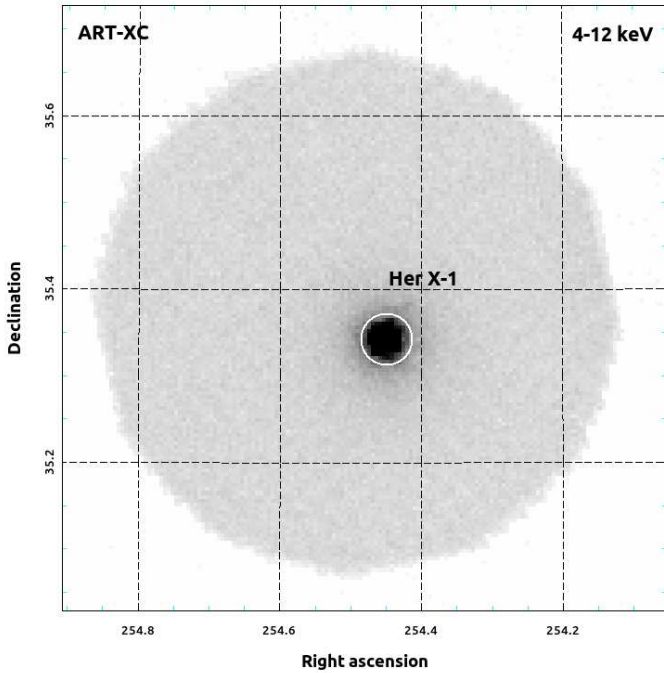


Fig. 1. ART-XC 4–12 keV image of the sky region around Her X-1.

ences therein). An extended hot corona above the accretion disk was detected during X-ray eclipses of Her X-1 in RXTE observations (Leahy 2015). In the first two all-sky surveys by the SRG/eROSITA telescope (0.4–10 keV, (Predehl et al. 2021)), the binary system was observed (about once every four hours for ~ 40 s) during the low states, where the neutron star is screened from the observer by the accretion disk, with a full exposure of 570 and 588 s accumulated over several days (Shakura et al. 2021). The SRG/eROSITA observations revealed an orbital modulation of the soft X-ray flux caused by scattering on a hot corona above the disk and on a hot optically thin corona above the X-ray-heated atmosphere of HZ Her.

This paper presents the results of dedicated continuous observations of the X-ray source Her X-1 by the Mikhail Pavlinsky ART-XC telescope of the SRG observatory in the 4–25 keV energy range during ≈ 1.94 days near the main X-ray source turn-on. The observations captured the end of the second low state, the X-ray eclipse, the main turn-on, and the X-ray flux increase in the main-on state beginning. These phases of the 35-day period are used to search for the expected modulation of the X-ray flux during nutation oscillations of the disk in the low state and for study features of the flux increase after the source’s turn-on.

2. ART-XC Telescope

The Mikhail Pavlinsky ART-XC telescope is one of two telescopes installed aboard the Spectrum-Röntgen-Gamma X-ray observatory. The SRG observatory was launched in 2019 from the Baikonur cosmodrome to the L2 libration point of the Sun-Earth system (Sunyaev et al. 2021).

The ART-XC telescope consists of seven co-directional identical X-ray modules. The mirror system provides a field of view of ~ 0.3 square degrees. The operating energy range of the ART-XC telescope is 4–30 keV, but the detectors can operate up to ~ 120 keV and the highest sensitivity is achieved at 4–12 keV. The time resolution of the telescope is $\sim 23 \mu\text{s}$ and the angular resolution is $\sim 53''$. Such parameters of the telescope make

it possible not only to survey large areas of the sky, but also to carry out a detailed spectral and temporal analysis of the radiation from individual objects (see Pavlinsky et al. 2021, for a more detailed description of the instrument).

3. Observations and data analysis

Dedicated observations of Her X-1 were carried out by the SRG/ART-XC telescope on August 25–26, 2023, near the moment of the main turn-on during 541th precession cycle according to the ephemerid (Postnov et al. 2013)

$$T_{\text{MJD}} = 42409.84 + 20.5 \times P_{\text{orb}} \times (N_{35} - 31), \quad (1)$$

where N_{35} is the precession cycle number, P_{orb} is the orbital period.

The ART-XC telescope data were processed using standard software ARTPRODUCTS v0.9 with the calibration data version CALDB 20230228; the photon registration times were adjusted to the solar system barycenter.

Figure 1 shows an image of the sky region around Her X-1 obtained with ART-XC telescope over the entire observational period. For further analysis only photons fell inside a circle with radius of $1/8$ around the source were used. The background was estimated by collecting photons from a circular region with a radius of $3/6$ on the detectors that did not overlap with the region in which the source photons were extracted.

Figure 2 shows the light curves of Her X-1 in two energy bands (4–12 keV, 12–25 keV) with a time resolution of 500 s. The figure shows that the entire X-ray light curve can be roughly divided into three main parts: (A) the pre-eclipse part, when the system is in the off (low) state and the neutron star is screened from the observer by the accretion disk; (B) the eclipse of the X-ray source by the optical star, where the observed X-ray flux reaches its minimum; (C) the post-eclipse part, when the source is opened to the observer. These stages will be discussed in more details below.

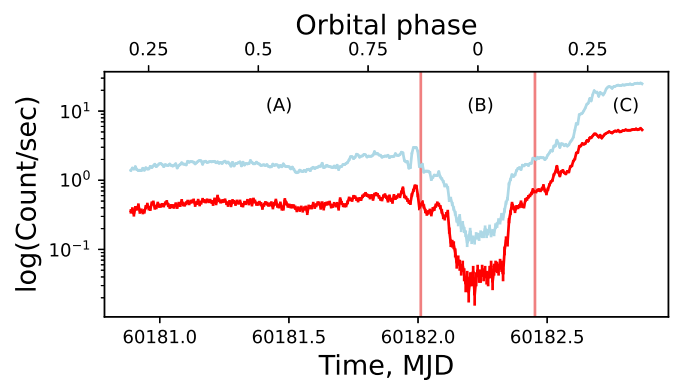


Fig. 2. ART-XC X-ray light curves of Her X-1 in two energy bands with a time resolution of 500 s (4–12 keV in blue and 12–25 keV in red). Zero orbital phase corresponds to the neutron star eclipse by the optical component.

Table 1. Best-fit parameter of the nutation model (3).

Energy range, keV	a_0 , counts/s	ϕ	k, counts/s/d	b, counts/s
4–12	0.38 ± 0.01	1.49 ± 0.02	0.85 ± 0.01	1.297 ± 0.008
12–25	0.088 ± 0.003	1.6 ± 0.04	0.24 ± 0.01	0.344 ± 0.004

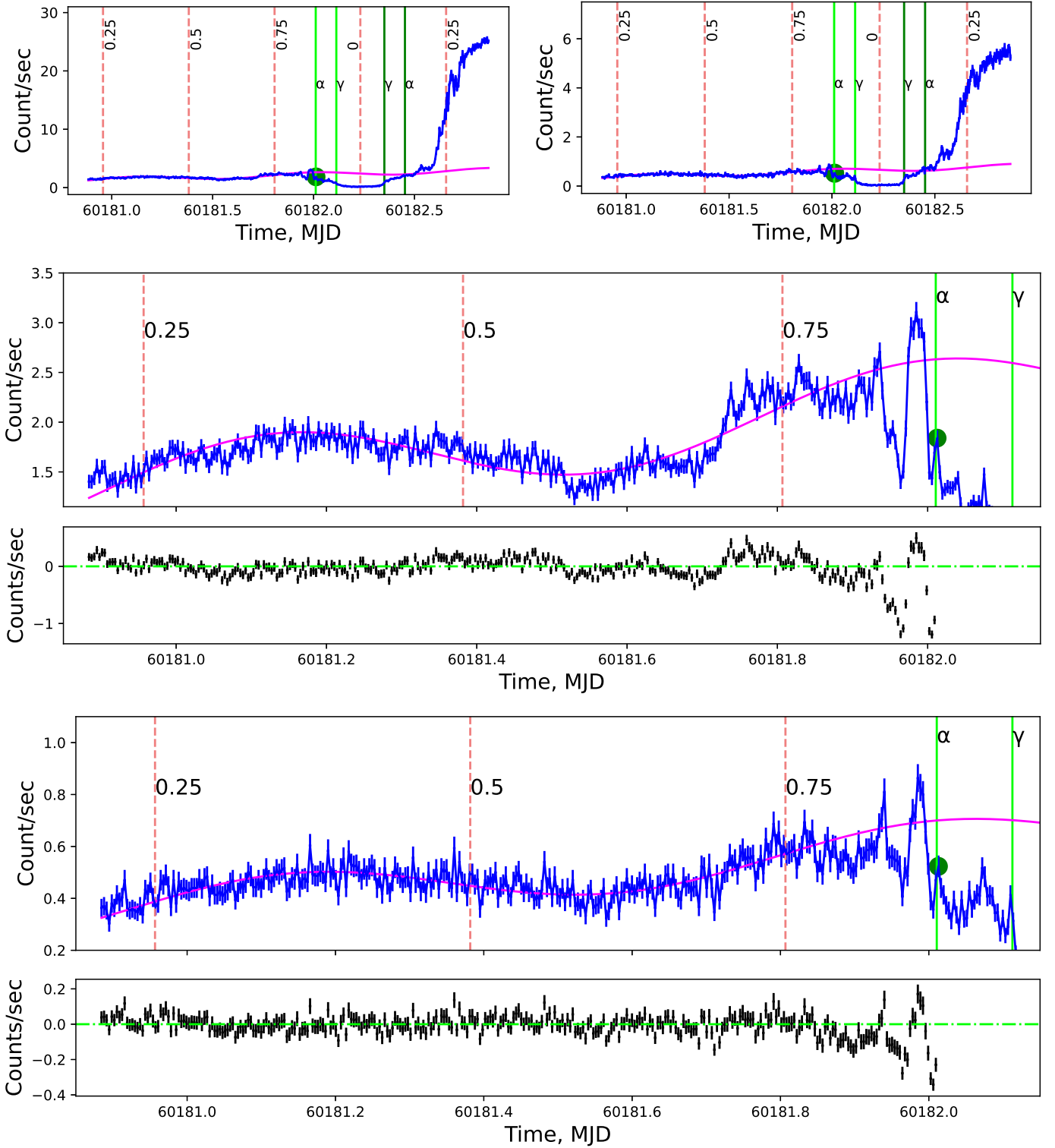


Fig. 3. ART-XC 4–12 keV (top left) and 12–25 keV (top right) light curves; enlarged pre-eclipse part of the 4–12 keV light curve (center) and enlarged pre-eclipse part of the 12–25 keV light curve (bottom). Blue errorbars correspond to 300s data binning, pink line corresponds to the best fit of the model parameters (3), and green solid circles correspond to the orbital phase up to which the model describes the observed light curve (the beginning of X-ray eclipse ingress). Light green vertical lines mark specific eclipse phases: α – the beginning of the accretion disk eclipse, γ – the neutron star eclipse. Dark green vertical lines mark the end of the corresponding eclipse phases. Red dashed vertical lines show specific orbital phases. Black errorbars show the model residuals.

As seen from Figure 2, the light curves are similar in both energy ranges, so they can be exemplified by the 4–12 keV light curve (where ART-XC has a larger effective area than in the 12–

25 keV range). The features on the 12–25 keV light curve generally coincide with those in the 4–12 keV range, except cases that will be considered separately. The orbital phases on the top

of Figure 2 are calculated using ephemerids from (Staubert et al. 2009).

Consider a geometrical model where the accretion disk centered on the neutron star to be a circle with radius $R_d \approx 0.7r_{L1}$ (Paczynski 1977), where $r_{L1} \approx a(0.5 + 0.227 \log_{10} q)$ is the distance between the compact star and the inner Lagrangian point L_1 (Frank et al. 2002), $q = M_x/M_o \approx 0.7$ is the binary mass ratio in Her X-1 (Abubekrov et al. 2008; Leahy & Abdallah 2014), a is the binary orbital separation, and the optical star is filling its Roche lobe $R_L(M_o) = af(\frac{1}{q})$, where $f(q) = \frac{0.49q^{2/3}}{0.6q^{2/3} + \ln(1+q^{1/3})}$ (Eggleton 1983). Her X-1/HZ Her is an almost edge-on binary system, so in this geometrical model we can estimate specific orbital phases of the beginning and end of eclipse of the accretion disk α and the neutron star γ by the optical star:

$$\begin{cases} \gamma = \pm \frac{1}{2\pi} \arcsin \frac{R_o}{a} \approx \pm 0.07 \\ \alpha = \pm \frac{1}{2\pi} \arcsin \frac{R_o + R_d}{a} \approx \pm 0.13. \end{cases} \quad (2)$$

(Note that these phases are almost insensitive to the assumed binary mass ratio $0.5 < q < 1$.) In this model, the beginning and end of eclipse of the accretion disk and neutron star, are symmetric with respect to zero orbital phase (full eclipse of the neutron star). Thus, the orbital phases α , γ , are 0.87, 0.93, and γ , $\alpha = 0.07$, 0.13, respectively (see Figure 3, top panels).

4. Results

4.1. Spectral analysis

Her X-1 spectra were constructed from ART-XC data using the XSPEC model `HIGHECUT(PowerLaw)+GAUSSIAN` (Staubert et al. 2020; Fuerst et al. 2013). Along the light curve the spectral parameters are found to remain approximately constant: $E_{\text{cut}} \sim 18$ keV, $E_{\text{fold}} \sim 8$ keV, photon index $\Gamma \sim 0.6$. Almost constant spectral parameters in the range of 0.5–7 keV across the 35-day cycle were also reported from the recent analysis of Her X-1 observations by AstroSat Soft X-ray Telescope (Leahy & Sharma 2024). However, a simple power-law model is sufficient to describe the spectrum in the X-ray eclipse. Moreover, the spectrum immediately after the eclipse up to the main turn-on of the source the spectrum becomes harder and an additional soft component appears (see below).

Figure 4 shows X-ray spectra in the X-ray eclipse (MJD 60182.15 – 60182.3, in green), in the pre-eclipse phase (MJD 60180.9 – 60181.5, in red), and in the main-on high state (MJD 60182.7 – 60182.9, in blue). In the post-eclipse phase before the main turn-on of the spectrum of a short hard peak (MJD 60182.5 – 60182.6) an additional soft component is required (in purple).

4.2. Analysis of post-eclipse X-ray spectrum

As mentioned above, for a short time (MJD 60182.5 – 60182.6) after the X-ray eclipse before the main turn-on, an additional soft component, not described by the `HIGHECUT(PowerLaw)+GAUSSIAN` model appears in the spectrum. This soft component can be described by the model of a black body with the temperature of $kT \sim 0.8$ keV (see Figure 5). At a source distance of $\sim 6.6 - 6.1$ kpc (Reynolds et al. 1997; Leahy & Abdallah 2014) the observed soft excess corresponds to radiation from a spot with a size of ~ 1 km

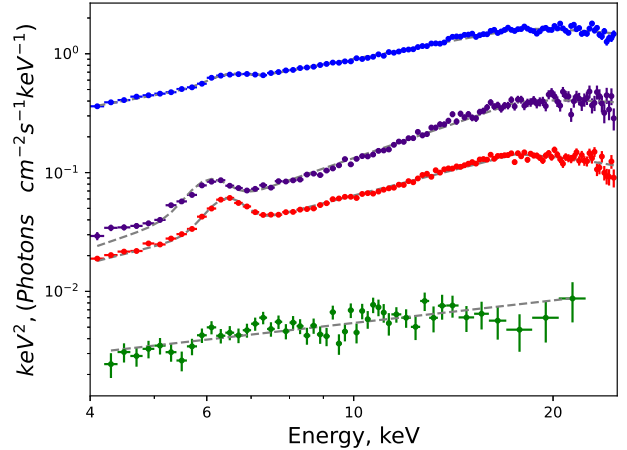


Fig. 4. ART-XC Her X-1 spectrum approximated by the `HIGHECUT(PowerLaw)+GAUSSIAN` model. From top to bottom: the main-on high state (MJD 60182.7 – 60182.9, in blue); the low state before the main turn-on after the X-ray eclipse when the neutron star is screened by the accretion disk (MJD 60182.5 – 60182.6, in purple); the low state before the X-ray eclipse (MJD 60180.9 – 60181.5, in red); the X-ray eclipse (MJD 60182.15 – 60182.3, in green).

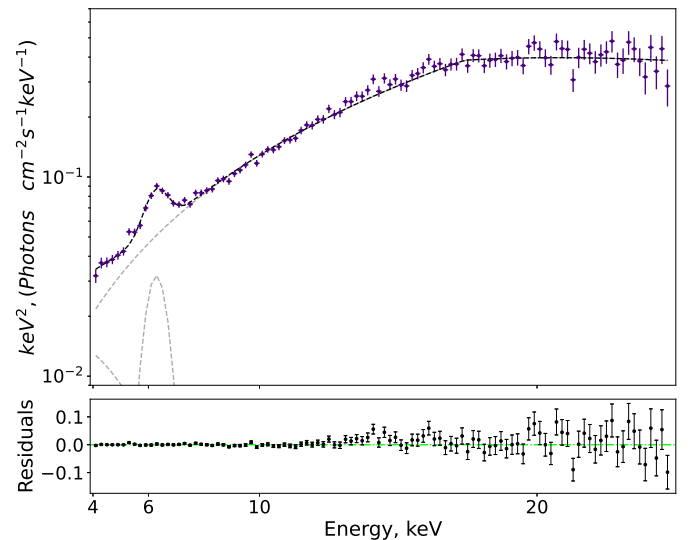


Fig. 5. (Top) Purple points – a hard spectrum in the low state (see Figure 4). Gray dashed lines indicate models: `HIGHECUT(PowerLaw)`, `GAUSSIAN`, `BLACKBODY`. The black dashed line is the total model. (Bottom) The difference between the observation points and the total model.

The emergence of this soft component for a short time before the main turn-on of Her X-1 can be related to the contribution of the hot spot from the interaction region between the gas stream from the inner Lagrangian point and the outer parts of the disk. The interaction of the infalling matter with the outer disk at $R_{\text{out}} \sim 1.6 \times 10^{11}$ cm produces shock with a temperature behind the front $kT \sim \frac{3}{16} m_p V^2$ (m_p is the mass of a proton). At characteristic ballistic velocities of the stream $V \sim 600 \frac{\text{km}}{\text{s}}$, this temperature is close to the temperature obtained from the spectral data.

Table 2. Model parameters of the ART-XC spectrum of Her X-1 after eclipse before the main-on (in purple in Fig. 4 and 5).

Parameter	Value	Error
E_{cut} (keV)	17.41	0.45
E_{fold} (keV)	10.44	1.09
Γ	0.01	0.05
norm_{pow}	0.0013	0.0002
E_{Fe} (keV)	6.23	0.07
σ_{Fe}	0.4	fixed
norm_{Fe}	0.0008	0.0001
kT	0.79	0.22
norm_{bb}	0.0004	0.0002

4.3. Analysis of the pre-eclipse light curve

In this section, we consider the pre-eclipse part of the light curve in the low state, when the emission from the central source is screened by the accretion disk. The residual X-ray flux during the eclipse can be due to scattering of the X-ray emission from the neutron star on the corona above the X-ray illuminated atmosphere of the optical star and on the disk corona as suggested by the analysis of the *SRG*/eROSITA observations of Her X-1 (Shakura et al. 2021). It is seen in Figure 2 that there is a marked increase in the flux near the orbital phase of 0.7 before the eclipse followed by the eclipse ingress.

The observed smooth variability of the X-ray flux in the off-state before the main-on seen in Fig. 3 may be tentatively related to the change of the disk tilt (wobbling) due to tidal precession (Klochkov et al. 2006). While seen only once, the characteristic time and phase of the observed variability are very close to the expected values for the disk wobbling model. The nutation period of the disk is $\frac{1}{P_{\text{nut}}} = 2 \times \frac{1}{P_b} - \frac{1}{P_{\text{pr}}}$. For Her X-1 $P_{\text{nut}} = 0.87$ days, or in units of cyclic frequency $\omega_{\text{nut}} \approx 7.2$ rad/d. In the wobbling disk model, the pre-eclipse part of the light curve should be modulated with the nutation period, with an additional term responsible for a much longer disk precession, which can be considered linear in a timescale of several days:

$$F = a_0 \times \sin(t \times \omega_{\text{nut}} - \phi) + k \times (t - T_0) + b. \quad (3)$$

Here t is the time at a given moment, T_0 is the time of the beginning of observations (fixed parameter), ω_{nut} is the nutation frequency, ϕ is the phase of nutation oscillations, b is the parameter specifying the flux in the zero phase of the modulation, k is the linear slope coefficient of the precession component, a_0 is the amplitude of the nutation modulation.

In the middle panels of Figure 3 we show the best approximation of the pre-eclipse part of the Her X-1 X-ray light curve with parameters given in Table 1. As can be seen in the bottom panels, there is a significant decrease in the registered emission before the eclipse, starting at about orbital phase 0.75, compared to the theoretical sine-like curve (purple line). Such a decrease in the flux before the eclipse ingress can be explained by the gas stream crossing the line of sight (the so-called pre-eclipse dip). As shown in Shakura et al. (1999), the pre-eclipse dip begins around orbital phase 0.8 in the precession phase before the main turn-on and smoothly transits into the X-ray eclipse ingress (see also Leahy & Igna (2011) for analysis of dips from the entire *RXTE*/PCA observations).

We also note that starting at about orbital phase 0.65 the 4–12 keV flux behaves less smoothly than the 12–25 keV flux. Near orbital phase 0.75 small quasi-periodic fluctuations of the

4–12 keV flux are observed with the characteristic time of $\approx 2000 - 3000$ s, which roughly corresponds to the Keplerian time of the orbit with a radius of 10^{10} cm around the neutron star. Since such pronounced peaks are not observed in the hard band, we can assume that such fluctuations of the X-ray emission are associated with the emission of a bright spot in the region of the accretion stream collision with the inner regions of a tilted disk (Shakura et al. 1999).

Our analysis suggests that the sine-like modulation observed by ART-XC in the pre-eclipse part of the Her X-1 X-ray light curve in the low state may be well explained by the wobbling disk model. Should this modulation be found persistent from longer observations (for example, phase-connected in both off-states), they would provide a direct observational manifestation of the nutation of the precessing accretion disk in the Her X-1/HZ Her system.

4.4. Analysis of the X-ray eclipse

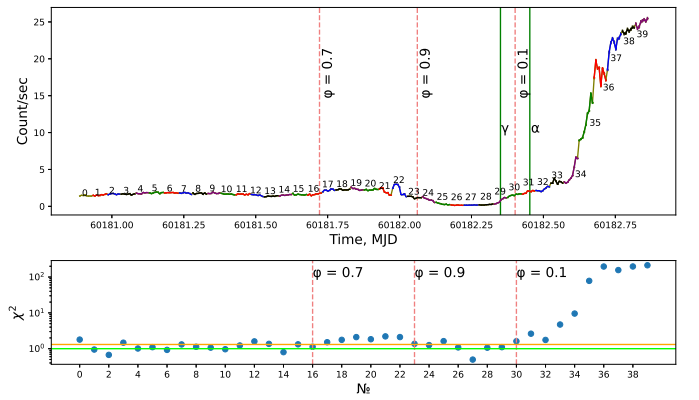


Fig. 6. Upper panel: The ART-XC 4–12 keV light curve of Her X-1 divided into 40 equal time intervals. Green lines mark the specific eclipse phases: $\gamma = 0.07$ is the opening of the neutron star by the optical star, and $\alpha = 0.13$ is the opening of the entire accretion disk by the optical star (see text). Bottom panel: Dependence of the χ^2 value of the deviations of the count rate in the X-ray pulse from the constant in each time interval; green line corresponds to $\chi^2=1$ and and orange line to 2σ -deviation of the pulsed flux from the constant.

Analysis of *RXTE* X-ray eclipses in Her X-1 was made previously by (Leahy 2015). In this section, the eclipsing part of the ART-XC light curve is considered. Figure 2 shows that the X-ray emission at the zero orbital phase does not disappear completely. In the analysis by (Leahy 2015), the residual emission in the X-ray eclipse was explained by scattering on a corona above the accretion disk. Here we consider an alternative explanation that this residual emission may be caused by the presence of an X-ray halo around the observer-facing part of the optical star eclipsing the X-ray source. Note that the light curve in the eclipse is asymmetric with respect to zero orbital phase, suggesting a complex shape of the tilted accretion disk producing asymmetric X-ray illumination of the optical star. As a result of the non-uniform heating of the the optical star atmosphere by the central X-ray source, the parts of the optically thin scattering corona above the heated up atmosphere of the star, visible during the X-ray eclipse ingress and egress, differ from each other.

To estimate the flux scattered by the optical star corona, we assume a ring-like X-ray halo around the optical star. Then we can estimate the ratio of the area of the ring-like halo visible at the orbital phase 0 to that of the hot corona above the atmo-

sphere of the optical star visible at the orbital phase 0.5, which was found in (Shakura et al. 2021). Considering the ratio of the corona thickness to the optical star radius $\frac{H}{R_{\text{opt}}} \approx 0.15$, the ratio of the radiation scattered by the corona to the total emission from an X-ray source in the energy range up to 8 keV near the orbital phase 0.5 can be estimated as $\frac{F_{\text{scat}}}{F_x} \sim 0.03$ (Shakura et al. 2021). The flux from the hot corona above the optical star at different orbital phases depends on its apparent area, from which we obtain an estimate for the expected flux ratio near orbital phase zero: $\frac{F_{\text{scat}}}{F_x} \sim 7 \times 10^{-3}$.

From the ART-XC data the observed ratio of the 4–12 keV flux during the X-ray eclipse near the zero orbital phase to the high-state flux is approximately $\frac{F_{\text{scat}}}{F_x} \approx (6.53 \pm 0.18) \times 10^{-3}$, which is in good agreement with the above model estimates.

4.5. The main turn-on time of the source

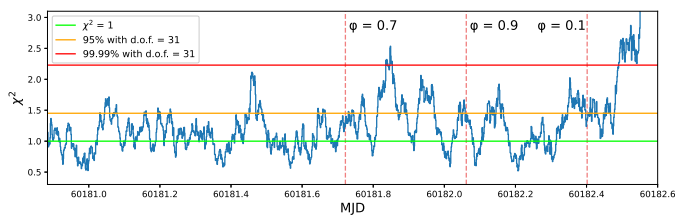


Fig. 7. χ^2 of the 4–12 keV pulse profile count rate deviations from constant constructed by the moving average method for time intervals of 4300 s with a 100 s shift. Green line corresponds to $\chi^2=1$, orange and red lines correspond to 2σ and 4σ flux deviations from constant, respectively.

Figure 6 shows that the main source turn-on – a sharp increase in the flux from Her X-1 – occurs much later than the neutron star’s exit from the eclipse by the optical star (phase $\alpha = 0.13$), which is expected in the geometrical model used. This means that the neutron star is still screened from the observer by the tilted accretion disk after the eclipse, and the turn-on happens near the orbital phase ~ 0.2 .

The moment of the pulsations appearance when the source is opened by the precessing disk is determined by the presence of a significant deviation of the pulse profile from constant. To determine the moment of the turn-on, the 4–12 keV light curve was divided into short equal-time intervals (≈ 4300 c), and in each time interval the count rates were convolved with the pulsation period of the neutron star (Figure 6). The pulsation period was determined from the last time interval (number 39 in Figure 6), when the neutron star is fully opened to the observer and the pulsating fraction of the emission is maximal, corrected for orbital motion: $P_{\text{spin}} = 1.2376986(1)$ s.

In the bottom panel of Figure 6, there are points exceeding 2σ deviation from constant pulse profile inside the interval (orange line). To test the significance of these outliers, a similar plot was constructed using the moving average method (Figure 7).

Figure 7 clearly shows that significant pulsations beyond the 4σ (red line) boundary was observed near the orbital phase ≈ 0.77 before the eclipse by the optical star. The observed 4–12 and 12–25 keV pulse profiles in the time interval MJD = 60181.848 – 60181.898 are shown in Figure 8 (black dots).

These profiles can be approximated by a characteristic sinusoidal trend (green curves in Figure 8). The profiles itself seems to have a small shift relative to the red pulse profiles obtained in the high state (interval #39). This may be caused by the fact

that before the eclipse the observed pulse profile was not seen directly from the neutron star, but, for example, represents reflected radiation on the tilted twisted accretion disk, which leads to a quasi-sinusoidal shape of the profile with an additional phase shift. However, we can not numerically estimate this phase shift or the distance to the reflecting region of the twisted disk with sufficient reliability because of the very different shape of the pulse profiles.

Thus we can conclude that the appearance of X-ray pulsations near the orbital phase 0.77 is not the direct emission of the source, since the pulse profile is strongly blurred and strongly affected by scattering on the corona of the accretion disk. Nevertheless, the fact that the pulse signal was detected before the main turn-on is very remarkable because it falls at the maximum of the sinusoidal flux fluctuation due to the disk nutation, which is geometrically favorable for seeing the scattered emission from a neutron star still covered by the disk at this precessional phase.

Figure 9 shows the pulse profiles near the main turn-on in the post-eclipse part. This figure clearly shows how the profiles change as the X-ray components are opened by the optical star: in the interval #30, where the neutron star is already open and the accretion disk is partially open, no pulsations are seen; in intervals #31–33, where the accretion disk emerges from the eclipse, smoothed profiles similar to those observed before the eclipse gradually appear; by intervals #34–35, characteristic Her X-1 profiles appear. This interval includes the moment of orbital phase 0.2, which we will consider to be the phase of the main X-ray source turn-on.

4.6. Modeling of the exponential rise

In this section, we discuss in more detail the time evolution of the X-ray flux in the post-eclipse light curve. Following (Kuster et al. 2005), we consider that the X-ray radiation from the neutron star reaches the observer, partially or completely absorbed and scattered in the disk corona, differently in different energy ranges.

The exponential flux increase after the turn-on can be modeled assuming that the influence of absorption is negligible, and the main role in the observed flux change is played by scattering in the disk corona associated with the change in the number of particles along the line of sight during the precessional motion of the disk: $F(t) = \tilde{F}e^{-\tau(t)}$. Taking into account the observed very sharp dependence of the logarithm of the flux on time, to approximate the X-ray light curve after the main turn-on we approximate the effective optical thickness by a function exponentially depending on time $\tau(t) = Ae^{-\frac{t-T_0}{b}}$. Then the flux rising is described as

$$F(t) = (F_0 - F_{\text{disk}}) \exp \left[-A \exp \left(-\frac{t - T_0}{b} \right) \right] + F_{\text{disk}}, \quad (4)$$

where T_0 is the initial time at which the flux growth starts, A is a dimensionless constant, b is a constant coefficient corresponding to the characteristic time of the flux change, F_0, F_{disk} are constant fluxes corresponding to contributions from the neutron star and the disk. The choice of such a function instead of, say, a polynomial approximation is also convenient because it provides the desirable asymptotics $F(t \ll T_0) \rightarrow F_{\text{disk}}$, $F(t \gg T_0) \rightarrow F_0$.

The plots for the best-fit exponential flux growth in the 4–12 and 12–25 keV ranges after the main Her X-1 turn-on are shown in Figure 10, respectively (see parameters in Table 3). It is seen that the model curve in general well describes the observed sharp flux increase during the opening of the neutron star by the precessing disk.

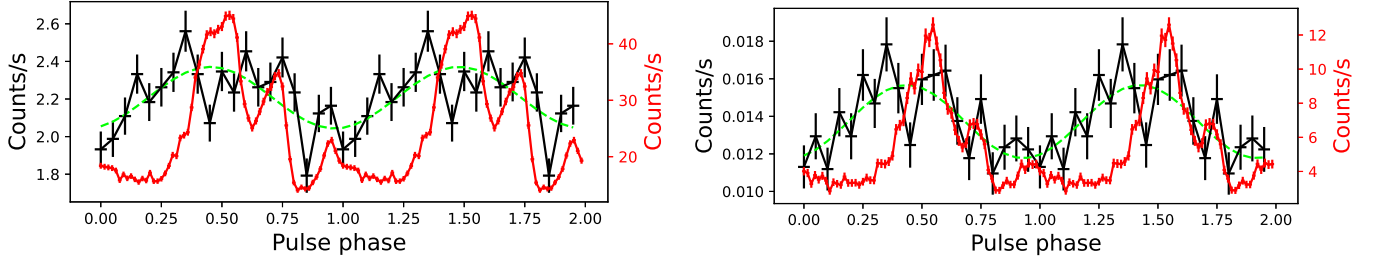


Fig. 8. Pulse profiles (4–12 keV on the left, 12–25 keV on the right) near the orbital phase 0.77 (MJD = 60181.848 – 60181.898; black color, scale on the left). Modeling of the pulse profile near the orbital phase 0.77 by sinusoidal curves (green color). For comparison, the pulse profiles after the main turn-on in time interval #39 in Figure 6 are shown (red color, scale on the right).

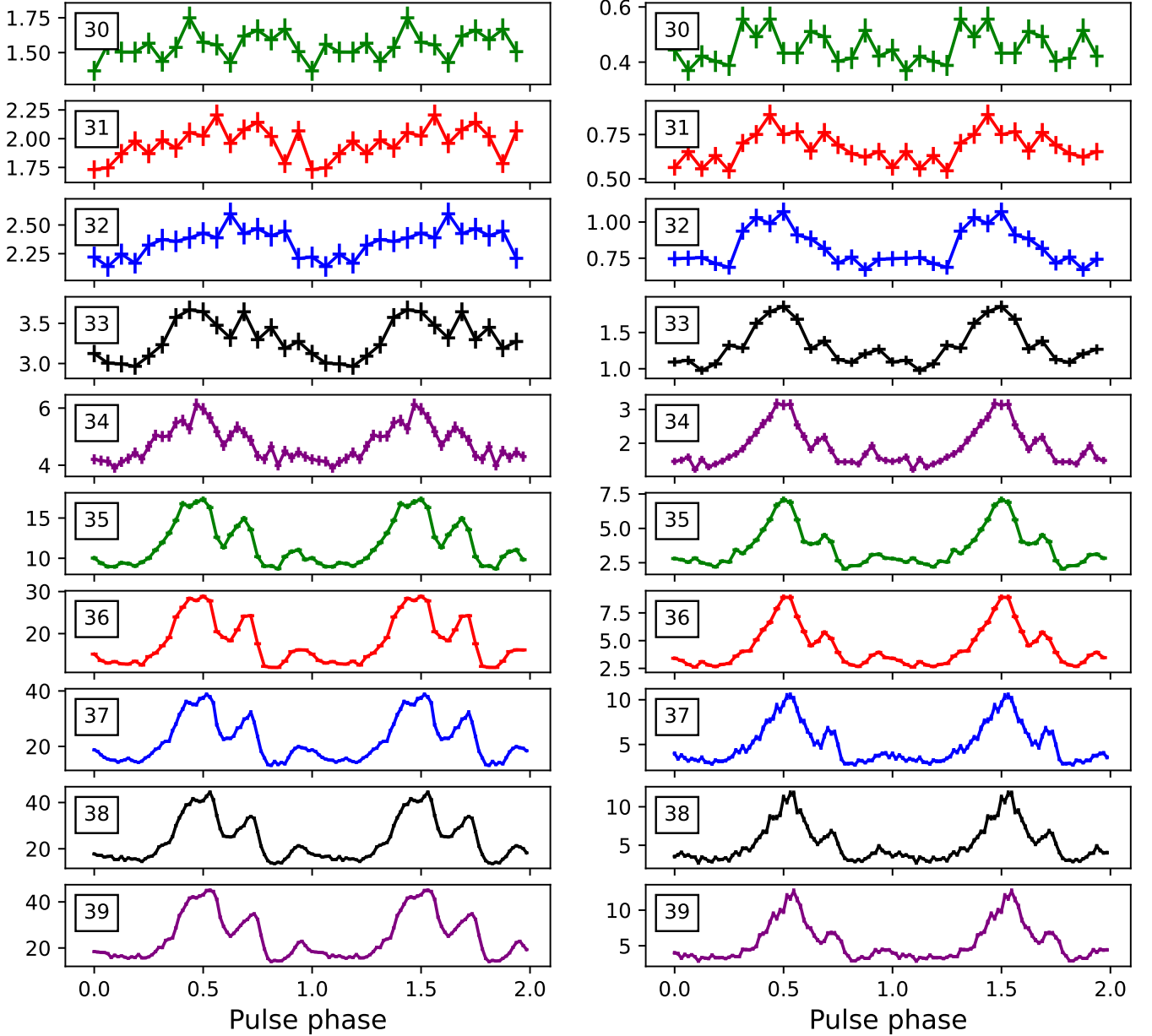


Fig. 9. (Left) Pulse profiles in the post-eclipse 4–12 keV (left) and 12–25 (right) light curves. Time intervals are numbered as in Figure 6.

The obtained parameters of the phenomenological model (4) are insufficient for unambiguous conclusions about a detailed physical structure of the scattering corona of the disk. However,

the model allows us to trace the general behavior of the light curve in both energy ranges, which is well described by scattering of radiation in the inhomogeneous corona of the accretion

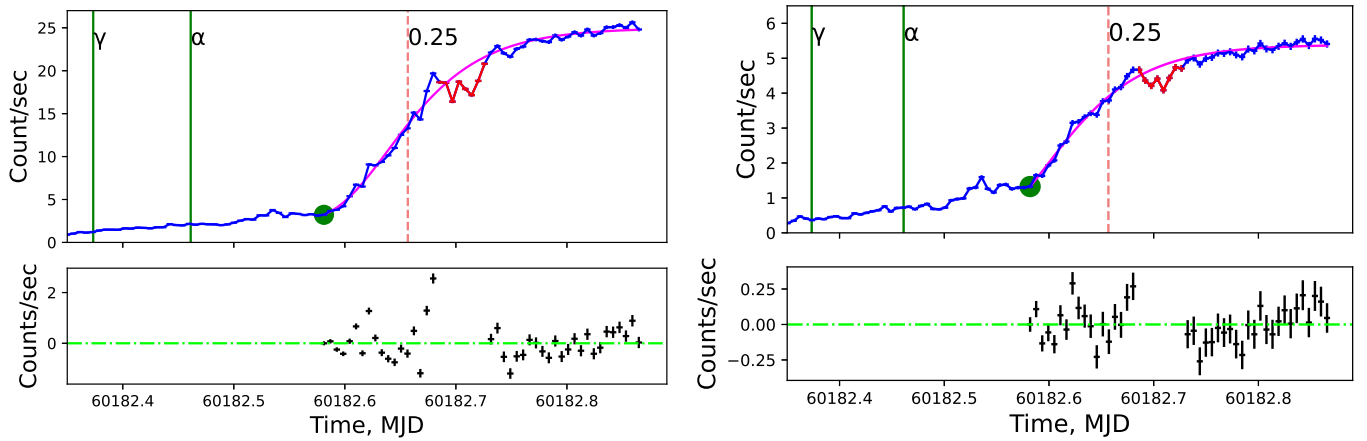


Fig. 10. Modeling of the 4–12 keV (left) and 12–25 keV (right) flux on the exponential rise after the main Her X-1 turn-on, errorbars correspond to 500 s data binning. Green filled circle marks the initial rise time of the X-ray flux T_0 (falls inside interval #34 in Figure 6), red dots are ignored as they correspond to the X-ray flux dip caused by the expected inhomogeneous gas stream from the Lagrangian point L_1 . In the bottom panel, black dots with errorbars show difference between the observed and model count rate.

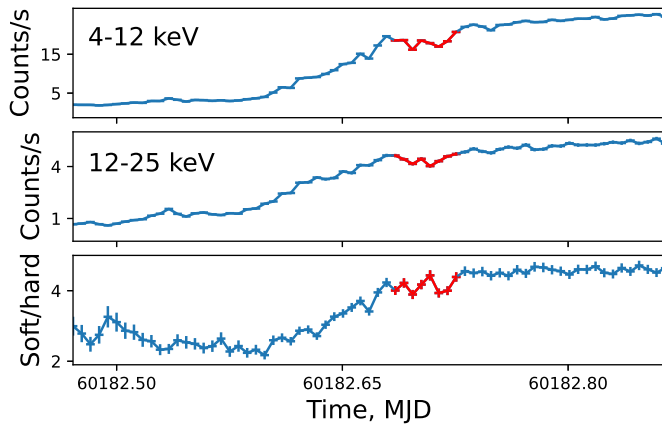


Fig. 11. Top panel: the 4–12 keV light curve of the exponential flux growth. Middle panel: the corresponding 12–25 keV light curve. Bottom panel: softness of the X-ray light curve during the emission growth after the main turn-on; red dots mark the X-ray dip as in Figs. 9–10.

Table 3. Parameter values of the exponential growth model (4)

Energy range, keV	A	b, d	$F_{\text{disk}}, \text{ counts/s}$
4–12	3.41 ± 0.07	0.048 ± 0.001	2.52 ± 0.05
12–25	1.82 ± 0.18	0.049 ± 0.002	0.54 ± 0.17

disk. The parameter b , responsible for the flux increase rate, has close values in both energy ranges, while all the difference in the flux growth is encoded in the time-independent parameter A (see Figure 11).

The X-ray hardness plot in the bottom panel of Figure 11 shows that during the phase of exponential flux growth the light curve behaves differently in different energy ranges, but the saturation of the flux increase occurs simultaneously in both ranges. This can also be seen in Table 2, where the value of parameter b is similar in different energy ranges, while the parameter A is very different. The harder emission up to the main turn-on is due to the preferential scattering of hard photons in a hot corona above the X-ray heated atmosphere of the optical star, as expected in the model of Her X-1 (Shakura et al. 2021).

In Figs. 3 and 10 in the post-eclipse light curve, a short peak before the onset of quasi-exponential growth near the orbital phase 0.18 (interval #33 in Figure 6) attracts attention. The peak is more pronounced in the hard range, which can also be seen in the spectrum. It is seen in Figure 9 that in the 12–25 keV energy range, the pulsations from the neutron star appear slightly earlier than in the 4–12 keV range, just in interval #33. Such a flux behavior can be explained by the fact that the registered radiation at this orbital phase may arrive not only scattered or re-reflected on the accretion disk, but also on the hot corona above the heated atmosphere of the optical star. It is known that the X-ray reflection albedo increases with the photon energy (Mescheryakov et al. 2011), which leads to a more pronounced reflected 12–25 keV pulse emission in interval #33 in Figure 6. However, we do not consider this moment to be the beginning of the main turn-on, since the neutron star must be still obscured by the tilted precessing accretion disk. Of course, to confirm that the appearance of this hard peak is spurious, new observations of Her X-1 at this phase are needed.

5. Conclusion

We present results of the Mikhail Pavlinsky ART-XC telescope observations of the eclipsing Her X-1/HZ Her X-ray binary system in the end of the second low state near the moment of the main source turn-on in the interval MJD = 60180.89 – 60182.87. A sine-like modulation of non-pulsating X-ray emission in the off state with a characteristic time of 0.87 days may be explained by tidal wobbling of the precessing accretion disk around the neutron star suggested by (Klochkov et al. 2006).

The 4–12 keV light curve shows a brief appearance of X-ray pulsations in the off state near the orbital phase 0.8 at the maximum of the proposed nutation variability, which may temporarily open the central source before the main-on (see Figure 6 in Klochkov et al. 2006). In our observations, the Her X-1 main-on is found to occur near the orbital phase 0.2, which is close to the phases 0.25 and 0.75 where the tidal nutation of the precessing accretion disk is mostly pronounced (Levine & Jernigan 1982; Katz et al. 1982). However, main turn-on times in Her X-1 have not always been found near these phases (Leahy & Dupuis 2010; Leahy & Wang 2020), and the model of tidal wobbling of accretion disk should be further checked by future observations.

A residual X-ray emission during the X-ray eclipse has been measured. The observed flux is consistent with a model of scattered radiation in an optically thin hot corona above the X-ray-illuminated photosphere of the optical star that was detected in Her X-1 observations with the *SRG*/eROSITA telescope (Shakura et al. 2021).

We analyzed the X-ray light curve after the main turn-on of Her X-1 and showed that it is possible to approximate the flux growth taking into account only scattering and time evolution of the column density associated with change in the number of particles along the line of sight when the source is being opened by the outer edge of the precessing accretion disk.

Acknowledgements. This work is based on observations with the Mikhail Pavlinsky ART-XC telescope, hard X-ray instrument on board the *SRG* observatory. The *SRG* observatory was created by Roskosmos in the interests of the Russian Academy of Sciences represented by its Space Research Institute (IKI) in the framework of the Russian Federal Space Program, with the participation of Germany. The ART-XC team thanks the Roscosmos State Corporation, the Russian Academy of Sciences, and Rosatom State Corporation for supporting the ART-XC telescope, as well as the JSC Lavochkin Association and partners for manufacturing and running the Navigator spacecraft and platform. The work was supported by the Minobrnauki RF grant 075-15-2024-647.

References

- Abubekurov, M. K., Antokhina, E. A., Cherepashchuk, A. M., & Shimanskii, V. V. 2008, *Astronomy Reports*, 52, 379
- Caiazzo, I., Doroshenko, V., Tsygankov, S., et al. 2022, in *American Astronomical Society Meeting Abstracts*, Vol. 240, American Astronomical Society Meeting #240, 246.03
- Cherepashchuk, A. M., Efremov, Y. N., Kurochkin, N. E., Shakura, N. I., & Sunyaev, R. A. 1972, *Information Bulletin on Variable Stars*, 720
- Crampton, D. & Hutchings, J. B. 1974, *ApJ*, 191, 483
- Eggleton, P. P. 1983, *ApJ*, 268, 368
- Frank, J., King, A., & Raine, D. J. 2002, *Accretion Power in Astrophysics: Third Edition*
- Fuerst, F., Grefenstette, B. W., Staubert, R., et al. 2013, *arXiv e-prints*, arXiv:1309.5361
- Gerend, D. & Boynton, P. E. 1976, *ApJ*, 209, 562
- Giacconi, R., Gursky, H., Kellogg, E., et al. 1973, *ApJ*, 184, 227
- Katz, J. I., Anderson, S. F., Margon, B., & Grandi, S. A. 1982, *ApJ*, 260, 780
- Klochkov, D., Staubert, R., Postnov, K., et al. 2008, *A&A*, 482, 907
- Klochkov, D. K., Shakura, N. I., Postnov, K. A., et al. 2006, *Astronomy Letters*, 32, 804
- Kolesnikov, D., Shakura, N., & Postnov, K. 2022, *MNRAS*, 513, 3359
- Kuster, M., Wilms, J., Staubert, R., et al. 2005, *A&A*, 443, 753
- Leahy, D. & Sharma, R. 2024, *Universe*, 10, 298
- Leahy, D. & Wang, Y. 2020, *ApJ*, 902, 146
- Leahy, D. A. 2015, *ApJ*, 800, 32
- Leahy, D. A. & Abdallah, M. H. 2014, *ApJ*, 793, 79
- Leahy, D. A. & Dupuis, J. 2010, *ApJ*, 715, 897
- Leahy, D. A. & Igna, C. 2011, *ApJ*, 736, 74
- Levine, A. M. & Jernigan, J. G. 1982, *ApJ*, 262, 294
- Lutovinov, A. A., Grebenev, S. A., Pavlinsky, M. N., & Sunyaev, R. A. 2000, *Astronomy Letters*, 26, 691
- Mescheryakov, A. V., Shakura, N. I., & Suleimanov, V. F. 2011, *Astronomy Letters*, 37, 311
- Paczynski, B. 1977, *ApJ*, 216, 822
- Pavlinsky, M., Tkachenko, A., Levin, V., et al. 2021, *A&A*, 650, A42
- Postnov, K., Shakura, N., Staubert, R., et al. 2013, *MNRAS*, 435, 1147
- Predehl, P., Andritschke, R., Arefiev, V., et al. 2021, *A&A*, 647, A1
- Reynolds, A. P., Quaintrell, H., Still, M. D., et al. 1997, *MNRAS*, 288, 43
- Schandl, S. & Meyer, F. 1994, *A&A*, 289, 149
- Scott, D. M., Leahy, D. A., & Wilson, R. B. 2000, *ApJ*, 539, 392
- Shakura, N. I., Ketsaris, N. A., Prokhorov, M. E., & Postnov, K. A. 1998, *MNRAS*, 300, 992
- Shakura, N. I., Kolesnikov, D. A., Medvedev, P. S., et al. 2021, *A&A*, 648, A39
- Shakura, N. I., Prokhorov, M. E., Postnov, K. A., & Ketsaris, N. A. 1999, *A&A*, 348, 917
- Staubert, R., Ducci, L., Ji, L., et al. 2020, *A&A*, 642, A196
- Staubert, R., Klochkov, D., & Wilms, J. 2009, *A&A*, 500, 883
- Sunyaev, R., Arefiev, V., Babyshkin, V., et al. 2021, *A&A*, 656, A132
- Tananbaum, H., Gursky, H., Kellogg, E. M., et al. 1972, *ApJ*, 174, L143
- Wijers, R. A. M. J. & Pringle, J. E. 1999, *MNRAS*, 308, 207